JOURNAL OF COMPUTATIONAL PHYSICS 119, 220–230 (1995)

Finite Element Numerical Modeling of Stationary Two-Dimensional Magnetosphere with Defined Boundary

M. D. KARTALEV AND M. S. KASCHIEV

Institute of Mechanics and Institute of Mathematics, Bulgarian Academy of Sciences, Sofia, 1113 Bulgaria

AND

D. K. KOITCHEV

Department of Mathematics, Sofia University "St. Kl. Ohridsky," Sofia, Bulgaria

Received September 7, 1993; revised September 20, 1994

A finite element numerical procedure is developed for two-dimensional modeling of stationary magnetosphere. The whole magnetic field is supposed to be a sum of given internal fields and a searched divergent-free and curl-free field of the magnetopause shielding current system. The boundary condition on the given boundary is the Neumann one on the magnetopause part of the computational region boundary and the Dirichlet condition on the segment part, closing this region at the tail. The algorithms used for automatic grid generation and grid transformation allow wide flexibility in determining the region shape and the assigned internal fields. Some numerical implementations not only demonstrate the method capabilities. In the frame of the two-dimensional approach these implementations could be considered as a tentative simulation of some typical features of magnetosphere magnetic field topology, which is intrinsically three-dimensional. The magnetopause geometry influence on the cusp inclination is shown. The impact of the northward and the flow-aligned field on dayside merging and tail asymmetry is aluminized. A two-dimensional approach to modelling the crosstail currents is proposed for the Earth-type and Uranus-type magnetospheres.

1. INTRODUCTION

The selection and formulation of the magnetosphere magnetic field mathematical model, as well as the selection of the mathematical approach to the solution of this model, is perhaps one of the fundamental problems of magnetospheric physics. It is well known that the solution and even the formulation of the complete self-consistent theoretical problem of finding the magnetospheric field and plasma topological features is practically not solved by now. That is why the efforts of studies are concentrated on the development of partially limited approaches, describing well enough the different essential features of the problem. The selection of the model in each particular case depends on the pursued goals, existing information, and estimation of the needed efforts.

One of the widely exploited useful approaches, developed by use of different mathematical means, is the stationary magnetosphere magnetic field model comprising given internal vector constituents and an unknown vector field, which is the object of determination. The given fields are usually induced by a dipole and some assigned current systems, simulating well-substantiated physical features in the magnetosphere cavity. The existence of a scalar potential—a harmonic function—is usually supposed for the vector field sought. In the case of the Earth magnetosphere a widely accepted approach for magnetosphere field determination is to seek it as a superposition of the Earth dipole field, the fields of the ring current, the crosstail currents, and the unknown magnetopause shielding current system. The determination of the potential of the field, inducted by the latter current system, results in a solution of a boundary value problem for the Laplace equation.

The development of such a type of models is reasonable because of the rather exact reflection of the common topological features of the magnetic field inside the magnetosphere and, under some appropriate suppositions, even the depiction of some features of the system: magnetosphere–solar wind. Explicitly or not, one supposes for that a maintaining of such features in the case of possible complete and detailed modeling of the real magnetosphere plasma and fields.

The models of this kind, existing in the literature, have distinct approaches, accuracy, and physical conformity of the boundary conditions, as well as the selection of mathematical techniques used in the solution.

As a rule, the boundary condition on the magnetopause is defined as a given distribution of the normal component of the magnetic field vector; i.e., the problem is usually a Neumann one for the searched field potential in the magnetosphere cavity [14, 12, 18]. In the closed magnetosphere models this normal component is supposed to be zero everywhere on the boundary. In the case of the open magnetosphere models, since an adequate description of the magnetopause structure is still missing,

0021-9991/95 $12.00

some reasonable normal component distributions are usually used to be set on the boundary. Such distributions are selected not only to be acceptable from a physical point of view, but they usually are chosen to be convenient from the point of view of mathematical formalism. This leads to some kind of restrictions. Avoiding such restrictions by introducing more universal mathematical approaches seems to be one of the worthwhile goals of further investigations of the problem.

A common aspect of the numerous mathematical formalisms used in the considerations of this problem in the literature is that the analytical solution is looked for mainly in the form of expansions of special functions, spherical harmonics, Bessel functions [18], parabolic harmonics [12], Fourier–Bessel integrals; then they are expanded over spherical harmonics with jointed Legendre polynomials [1], and so on.

The magnetosphere boundary is usually supposed to be defined first in searching for the internal field.

The goal of this paper is the development of a numerical mathematical procedure for solving the problem of the magnetic field potential in a stationary magnetosphere. The procedure proposed here is supposed to be more flexible and accurate in the following aspects:

- Avoiding restrictions on the given shape of the magnetosphere boundary;
- Minimizing restrictions on the given boundary conditions;
- Being flexible in the construction of solutions as a superposition of arbitrary, but physically acceptable (including non-harmonic) functions, describing internal fields;
- Providing options for reaching some degree of self-consistency among the influences of the physical phenomena, described by the functions mentioned;
- Being universal enough as to permit the description of different astrophysical objects, different kind of magnetospheres, as well as cavities of non-magnetic planetary bodies.

The two-dimensional approach here is considered as a first step in the problem analysis. First, this is an essential methodological experiment, performed before going to the three-dimensional problem. At the same time the two-dimensional consideration could lead to some physical conclusions as well. These could be some global features of the system magnetosphere—solar wind, important details of the magnetic field topology in the midday–midnight magnetosphere cross section, and so on. Certainly, it is well known that magnetosphere dynamics is intrinsically a fully three-dimensional problem and that is why any physical conclusion, derived by the two-dimensional approach has to be considered very carefully and tentatively.

The numerical finite element method is used in this paper to achieve the above-mentioned goals. The basic physical assumptions for the described magnetospheres and the general mathematical formulation of the problem are presented in Section 2. Section 3 is devoted to formulation of the numerical problem, description of the numerical procedure for its solution, as well as to some auxiliary numerical procedures used for the presentation of the solution. Some numerical results are presented in Section 4. Section 4.1 contains several examples of solutions for open and closed magnetospheres of the Earth's type, demonstrating the capabilities of the numerical procedure in simulation of typical features of magnetic field topology. In particular, a concrete model for the crosstail current is chosen for this purpose. In Section 4.2 the numerical method is used for modeling a "pole-on" two-dimensional cross section of the Uranus magnetosphere that is possible in a certain orbit position. This includes a simplified presentation of a cylindrical tail current sheet.

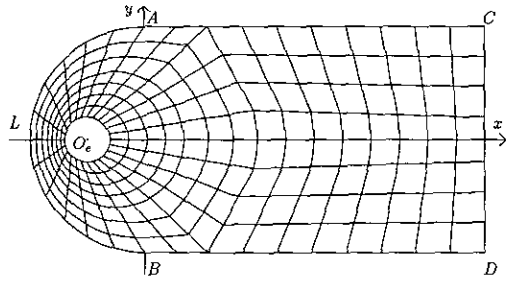

FIG. 1. A basic computational region Ω (here with internal circular cut G with radius 0.2, centered in point $O_c(-0.5, 0)$), used in a numerical example in Section 4.1.1 for drawing the magnetic field lines. The coordinates of the typical points are: $A(0, 1)$, $B(0, -1)$, $L(-1, 0)$, $C(3, 1)$, $D(3, -1)$. An automatically generated grid (Section 3.2) is shown in the figure.

2. FORMULATION OF THE PROBLEM

The magnetospheric magnetic field is searched as a sum of the assigned constituent fields and an unknown vector field in a defined geometrically closed domain with given boundary conditions.

As a simplified geometry of the model magnetosphere, a two-dimensional fixed domain Ω with boundary $\partial\Omega = \gamma \cup \sigma$ (Fig. 1) is considered. Here Ω is limited domain in $\mathbb{R}^2$; $\gamma = CALBD$ corresponds to the magnetopause or ionopause border, separating the magnetosphere from the solar wind flow region (magnetosheath) and $\sigma = CD$ is a section limiting the domain of the solution. It is enough for the following consideration that these boundaries be partially smooth curves in $\mathbb{R}^2$. The numerical approach will not impose any principal restrictions on the domain geometry.

Following [18], a geometry, shown in Fig. 1, is chosen for the numerical implementations in this paper. Here ALB is a semicircle with center ($x = 0$, $y = 0$), BD and AC are sections of straight lines, CD is a straight section, perpendicular to them.

A length scale, in which $AB = 2.0$, is used further. An existence of internal cuts in Ω is admitted, allowing, for instance, isolating some of the singularities. In Fig. 1 such a cut is circle G, introduced usually around the dipole singularity.

An assumption is made that the magnetic field inside Ω is stationary and divergent-free. The whole magnetic field $\mathbf{B}$ is a sum of different constituents,

$$\mathbf{B} = \mathbf{B}_s + \sum_{i=1}^{M} \tilde{\mathbf{B}}_i \tag{1}$$

where $\tilde{\mathbf{B}}_i$ are M, given for physical reasons, divergent-free vector fields, which may possess or not corresponding harmonic potential functions. The solution $\tilde{\mathbf{B}}_s$ is "fitted" to these given fields by conforming the boundary conditions in a way which may be specific for each given field. This conforming could be quite essential, especially concerning the boundary segment σ.

The sought part of the field $\mathbf{B}_s$ is supposed to be divergent-free and curl-free,

$$\operatorname{div} \mathbf{B}_s = 0, \quad \operatorname{rot} \mathbf{B}_s = 0, \tag{2}$$

and therefore a corresponding harmonic scalar function, field potential U, exists:

$$\nabla U = \mathbf{B}_s \tag{3}$$

$$\Delta U = 0. \tag{4}$$

The boundary condition for U on γ is the distribution of the normal to this boundary magnetic field component $(\mathbf{B}_s, \mathbf{n}) = \partial U/\partial n$ ($\mathbf{n}$ is the outward normal unit-vector of γ). This is a quite usual supposition for similar approaches.

Such a condition is based on the general supposition that the distribution of the normal component of the whole magnetic field on γ could be given as function $\tilde{\psi}$, defined by additional physical reasons, which are not a subject of discussions in this paper:

$$(\mathbf{B}, \mathbf{n}) = \tilde{\psi} \quad \text{on } \gamma. \tag{5}$$

Referring to the searched solution $\mathbf{B}_s$, condition (5) turns to

$$(\mathbf{B}_s, \mathbf{n}) = \tilde{\psi} - \sum_{i=1}^{M} (\tilde{\mathbf{B}}_i, \mathbf{n}) \quad \text{on } \gamma, \tag{6}$$

or in terms of the potential function that are supposed to exist for $\mathbf{B}_s$ (but not necessarily for $\mathbf{B}$),

$$\frac{\partial U}{\partial n} = \tilde{\psi} - \sum_{i=1}^{M} (\tilde{\mathbf{B}}_i, \mathbf{n}) \quad \text{on } \gamma. \tag{7}$$

The boundary conditions on the boundary segment σ need additional consideration and admit different variants. It is undesirable, however, to prescribe the normal field component on σ, since this would lead to boundary condition restrictions for the internal Neumann problem. In the numerical implementations in this paper the Dirichlet boundary conditions are put on σ,

$$U = \varphi \quad \text{on } \sigma, \tag{8}$$

which is convenient mathematically and appears to be reasonable physically.

In this way the formulation of the problem for $\mathbf{B}_s$ is given by Eqs. (4), (7), (8) and the whole field distribution is given by (1), (3).

Aiming to satisfy, at least partially, some physically grounded self-consistency, besides the above-described straightforward formulation, additional possibilities are foreseen in our problem consideration. In addition to the solution $\mathbf{B}_s$, fitted to all given fields $\tilde{\mathbf{B}}_i$, some intermediate solutions could be considered as well, fitted only to some part of the given fields $\tilde{\mathbf{B}}_i$, regarded as a firmly fixed one,

$$\mathbf{B}_m = \mathbf{B}_{s_m} + \sum_{i=1}^{m} \tilde{\mathbf{B}}_i \quad \text{in } \Omega; \, m < M. \tag{9}$$

It is implied that the determination of some of the remaining given field ingredients ($\tilde{\mathbf{B}}_i$, $i = m + 1, \ldots, M$) could be affected by $\mathbf{B}_{s_m}$. As an example, the disposition and even some parameter's values of the crosstail current system of the Earth's magnetosphere could be settled in accordance with the field topology previously obtained excluding this system. A similar settling could be admitted to the boundary condition on σ as well.

The latter considerations make reasonable the idea to divide, if necessary, the solution procedure into a sequence of several solution steps, each of them "complicating" the whole solution, taking into account one or several new given internal field ingredients. At each step the problem (4), (7), (8) is solved, summing in (9) from 1 to m, where $m \leq M$.

Note that a proper iteration procedure could be useful in some cases at the certain solution step in order to achieve self-consistency. Such a procedure is implemented in the numerical example in Section 4.1.2.

3. NUMERICAL PROCEDURE

A finite element method is applied for numerical solution of the problems discussed above. The considered problem variants, as well as each step of the possible iteration procedures mentioned, lead to the solution of the following boundary value problem:

$$\begin{aligned} &\Delta U(x, y) = 0; (x, y) \in \Omega, U \in C^2(\Omega) \cap C^1(\Omega \cup C^0(\Omega \cup \sigma) \\ &\frac{\partial U(x, y)}{\partial n} = \psi(x, y); (x, y) \in \gamma \\ &U(x, y) = \varphi(x, y); (x, y) \in \sigma. \end{aligned} \tag{10}$$

Let us first consider the weak formulation of the problem (10) (Galerkin scheme). We denote the set $H_E^1(\Omega) = \{w \in W_2^1(\Omega): w|_\sigma = \varphi\}$ and the space $H_{0E}^1(\Omega) = \{w \in W_2^1(\Omega): w|_\sigma = 0\}$. The weak formulation consists in seeking function formulation. The problem is to find

$$U \in H_E^1(\Omega), \quad a(v, U) = f(v) \quad \text{for each } v \in H_{0E}^1(\Omega), \tag{11}$$

where

$$a(w_1, w_2) = \int_\Omega \nabla w_1 \nabla w_2 \, d\Omega, \quad f(w) = \int_\gamma w\psi \, d\gamma. \tag{12}$$

3.1. Finite Element Computational Scheme

A standard finite element computational scheme [13, 2] is applied. Present Ω as $\Omega = \bigcup_{e\in\omega} e$, where e are curvilinear quadrangles, satisfying the conditions for consistency [13]. Here we designate as ω the totality of these quadrangles, which are accepted to be eight-node isoparametric cirendipe finite elements [2]. The nodes in each element are the apexes of the quadrangles and the middles of their sides. Denote $\{(x_i, y_i)\}_{i=1}^N$ as the totality of all nodes so-defined.

The use of the 8-node isoparametric elements here is accepted for several reasons. This approach provides the needed smoothness of the solution approximation inside the elements, which is important particularly in drawing field lines (Section 3.3). This type of elements also provides more precise approximation of curvilinear boundaries. This could be important when there are strong gradients of the solution near the curvilinear boundary or for the boundaries with complicated geometry (e.g., sharp corners around the cusp in possible future studies).

Denote $\{\Phi_i(x, y)\}_{i=1}^N$ the corresponding basic functions. Denote a set

$$S^h(\Omega) = \left\{ u^h = \sum_{i=1}^N c_i\Phi_i : (c_1, c_2, \ldots, c_N) \in \mathbb{R}^N, \right. \\ \left. c_i = u^h(x_i, y_i) = \varphi(x_i, y_i) \text{ for } (x_i, y_i) \in \sigma \right\} \tag{13}$$

and a space

$$S_0^h(\Omega) = \left\{ v^h = \sum_{i=1}^N \tilde{c}_i\Phi_i : (\tilde{c}_1, \tilde{c}_2, \ldots, \tilde{c}_N) \in \mathbb{R}^N, \right. \\ \left. \tilde{c}_i = v^h(x_i, y_i) = 0 \text{ for } (x_i, y_i) \in \sigma \right\}. \tag{14}$$

The problem (11) is considered in $S^h(\Omega)$; i.e., one is looking for $U^h \in S^h(\Omega)$, such that

$$a(v^h, U^h) = f(v^h) \quad \text{for each } v^h \in S_0^h(\Omega). \tag{15}$$

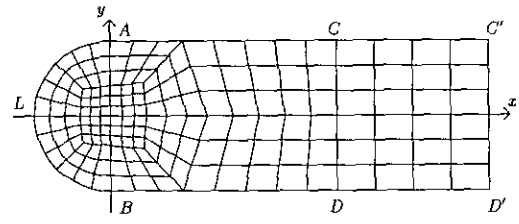

FIG. 2. Accepted geometry of the basic computational domain $\Omega = CALBD$. The extended domain $C'ALBD'$ is used in the realized computational procedures (Section 4). The coordinates of the typical points are: $C'(4.5, 1)$, $D'(4.5, -1)$. This is a typical finite element grid, used in the numerical examples (Section 4).

Applying a straightforward procedure one can turn (15) into a linear algebraic system with a semi-definite symmetric matrix.

The following error estimates are valid [13],

$$\|U - H^h\|_{1,\Omega} \le O(h^2),$$

where U is the solution of (11), U^h is the solution of (15); $h > 0$ is a majorant of the linear scale of the elements from ω, and

$$\|v\|_{1,\Omega} = \left\{ \int_\Omega [(\nabla v)^2 + v^2] \, d\Omega \right\}^{1/2}.$$

The computational techniques, described in [2] are used here in creating the linear algebraic system.

Gauss three-point quadratures are used for the computation of the integrals (stiffness matrix elements) over each finite element. The Cholezki expansion algorithm [13] is used in the numerical solution of the linear system, owing to the fact that its matrix is a sparse one [8].

3.2. Finite Element Grid Generation

An automatic grid generation algorithm, described in [5, 4], is used. The main computational domain is divided "manually" into a system of big curvilinear quadrangles (superelements) satisfying the conditions for consistency. Then the numbers of subintervals over each side of each quadrangle are assigned. These numbers could be different on different sides. The grid inside quadrangles is constructed automatically. The grid generation algorithm ensures satisfying the conditions for consistency.

The needed features of the grid are defined by the superelement construction. An appropriate renumbering of the nodes is performed in a way that minimizes the stiffness matrix trace. This helps the application of the Cholezki expansion mentioned.

A typical finite element grid, used in the numerical examples in the present study (Section 4) is drawn on Fig. 2. the coordinates of the typical points are: $A(0, 1)$, $B(0, -1)$, $L(-1, 0)$, $C(3, 1)$, $D(3, 1)$, $C'(4.5, 1)$, $D'(4.5, -1)$.

3.3. Drawing Field Lines of the Vector Field, Given in Finite Element Approximation

The vector lines of the whole magnetic field **B**, (1) in parametric form $x = x(t)$, $y = y(t)$ are given by the system

$$\frac{dx}{dt} = \frac{\partial U}{\partial x} + \tilde{B}_x, \quad \frac{dy}{dt} = \frac{\partial U}{\partial y} + \tilde{B}_y, \tag{16}$$

where $\tilde{\mathbf{B}} = (\tilde{B}_x\, \tilde{B}_y)^T = \sum_i \tilde{\mathbf{B}}_i$ is the entire given part of the field.

It is important to note that $\tilde{\mathbf{B}}$ could have singularities in Ω, which is the reason for considering (16) in its subdomain $\Omega_1 \subset \Omega$, which is such that the field $\tilde{\mathbf{B}}$ is limited in Ω_1. In terms of the next section, for example, Ω_1 is the domain with a circular cut around the singularity of the dipole field. This leads to a corresponding partition of Ω_1 to a grid ω_1 of finite elements that are generally not congruent to ω.

A specific task in the problem considered here is the possible necessity of replacement of the function v^h, given over the finite element coverage ω of Ω by other function, given over ω_1 of Ω_1. Practically, the problem of transition into the other grid results in determining the geometric locus of the given node (x_*, y_*) of ω_1 in ω, i.e., finding the element $e \in \omega$ containing this node; then resolving in point (x_*, y_*) the local map on $e \in \omega$ $(x = x(\xi, \eta), y = y(\xi, \eta))$ with respect to (ξ, η) by use of the Newton method; and finally in determining from $v^h(x, y)|_e = v^h(x(\xi, \eta), y(\xi, \eta))$ the value of v^h in this node in ω_1.

Consider (16) locally over each element $e \in \omega_1$ as soon as the sought function $U^h \in S^h(\Omega)$ is not smooth on the boundary of the elements. Then over e, in the variables (ξ, η), the system takes the form

$$\frac{d\xi}{dt} = F_1^e(\xi, \eta), \quad \frac{d\eta}{dt} = F_2^e(\xi, \eta) \tag{17}$$

This system of differential equations is solved using the Runge–Kutta method with error $O(|\tau|^4)$, where τ is a step of t. F_1^e and F_2^e are not defined explicitly and their values in (ξ, η) have to be searched at each step of the transformation of (16) in (17).

The procedure, developed for finding the field line consists in the following steps:

(i) Selection of the starting point (x_0, y_0) and determining the element $e \in \omega_1$ which is such that $(x_0, y_0) \in e$.

(ii) Resolving in (x_0, y_0) the local map on $e(x = x(\xi, \eta), y = y(\xi, \eta))$ with respect to (ξ, η) by use of the Newton method. Determination of (ξ_0, η_0).

(iii) Solving over e the system (17) using Runge–Kutta with initial condition $\xi = \xi_0$ and $\eta = \eta_0$ and step τ to t. Following the integral curve to the point Z of its "entering" the next element e^* (this curve crosses the boundary at e at Z).

(iv) Solving (17) in the new element with initial point Z.

(v) Following the same procedure till leaving Ω_1.

(vi) Implementation of a similar procedure starting again from $(\xi_0, \eta_0) \in e$ with a step $-\tau$.

4. SOME NUMERICAL REALIZATIONS

The results of some numerical experiments expounded here, despite the insufficiency of the two-dimensional approach, demonstrate well enough the perspectives of the scheme developed. The possibility for quantitative study of some effects of the magnetospheres topology, obtained by qualitative reasons or using some other model research, is shown.

The choice in the concrete numerical implementations of the function $\tilde{\psi}$, a distribution of the normal to the magnetosphere boundary γ component of the whole magnetic field **B**, deserves some additional comments. No formal mathematical restrictions are imposed on this function here (if $\tilde{\psi} \in C^0(\gamma)$). Presumably such a flexibility could be quite useful when a better physically justified distribution (for example, from the magnetopause structure study) is available. The accent in the implementations described here, however, is not on the physical approach, but mainly on the demonstration of the numerical procedure.

The next simplified, but flexible enough, determination of the distribution $\tilde{\psi}$ is accepted in these implementations:

$$\tilde{\psi}(x, y) = \begin{cases} (\mathscr{C}_L - \mathscr{C}_A) \sin\left(\arctan\dfrac{y}{x}\right) + \mathscr{C}_L & \text{on } LA, \\ (\mathscr{C}_B - \mathscr{C}_L) \sin\left(\arctan\dfrac{y}{x}\right) + \mathscr{C}_L & \text{on } LB, \\ \mathscr{C}_A + \alpha_A x & \text{on } AC, \\ \mathscr{C}_B + \alpha_B x & \text{on } BD, \end{cases} \tag{18}$$

$$\mathscr{C}_X = \mathscr{C}_X^* \mathscr{B}_{L\tau}; \quad (X = A, B, L).$$

The constants $\mathscr{C}_L, \mathscr{C}_A, \mathscr{C}_B$ are the values of the magnetic field vector normal component in the points L, A, B correspondingly (positive $\mathscr{C}_X$ corresponds to the outward field normal direction; negative $\mathscr{C}_X$, to the inward one). The coefficients α_A, α_B characterize the normal component variation from A to C and from B to D. The units for the constants $\mathscr{C}_X$ are scaled to $\mathscr{B}_{L\tau}$, which is equal to the magnitude of the whole field at the subsolar point L (Figs. 1, 2), found in the approach of a vacuum-closed magnetosphere (Section 4.1.1).

All these constants are to be made firm in each numerical example.

Under the presumption that the magnetic field vector tends asymptotically to be parallel to Ox downtail, the following scheme for settling the conditions on CD is adapted here.

The domain $CALBD = \Omega$ is extended to $C'ALBD' = \Omega^*$, obtained by lengthening BD and AC to BD' and AC'; $(D'C' \parallel DC)$. The domain Ω^* is divided into finite elements,

TABLE I

Dependence of Υ upon the Length of Ω^* Extension in the Case Described in Section 4.1.1 (Fig. 3) by the Step of Extension χ Equal to 0.5

Iteration number	1	2	3	4	5	6	7
CC'	2.0	2.5	3.0	3.5	4.0	4.5	5.0
Υ		1.00000	0.228402	0.043103	0.010087	0.001947	0.000799

maintaining the partition ω of the common domain Ω. The finite elements of the $\Omega^*\backslash\Omega$ are constructed relatively larger.

Then the considered mixed boundary value problem is solved numerically, making the Dirichlet condition firm on $C'D'$ as

$$U = -\tilde{U}_1, \tag{19}$$

where $\tilde{U}_1$ is the dipole potential, as well as setting the Neumann conditions for the segments CC' and DD' to be the same as determined from (18) in the points C and D, respectively.

Having the latter solution, the corresponding distribution $\mathbf{B}_s$ of grad U on CD is obtained to be analyzed. A convenient step χ for increasing $CC' = DD'$ is used. Denote Ω^{k*} to be the domain Ω^*, corresponding to the kth iteration in lengthening BD and AC. Repeating the iteration procedure, taking larger extensions of $CC' = DD'$, one finds the asymptotic behavior of the distribution $\mathbf{B}_s$ by means of the convenient estimation

$$\Upsilon = \frac{\max_{CD} |\mathbf{B}_s^{k*} - \mathbf{B}_s^{(k-1)*}|}{\max_{CD} |\mathbf{B}_s^{2*} - \mathbf{B}_s^{1*}|}, \tag{20}$$

where $\mathbf{B}_s^{k*}$ means the $\mathbf{B}_s$, corresponding to kth iteration of Ω^*.

Table I presents the dependence of Υ upon the length of Ω^* extension in the case described in Section 4.1.1 (Fig. 3). The step of the extension χ is equal to 0.5 in this case. In all of the examples considered here $\Upsilon < 0.01$ was achieved for CC' no longer than 1.5 AC.

4.1. An Open Two-Dimensional Model of the Earth Magnetosphere

The construction of a two-dimensional magnetic field model of the Earth-type magnetosphere, containing a dipole field and, in addition, a given model of a crosstail current field, is a simplified but informative enough numerical example. This is a comprehensive concrete illustration of the basic capabilities of the numerical procedure.

The two-dimensional dipole field with potential $\tilde{U}_1$ is accepted as a first constituent $\tilde{\mathbf{B}}_1$ of the whole field

$$\tilde{U}_1 = -\frac{(\mathbf{m}, \mathbf{r})}{2\pi\mathbf{r}^2}, \tag{21}$$

where $\mathbf{m}$ is the dipole moment and $\mathbf{r}$ is the radius-vector.

A generalization of a two-dimensional variant of the formula proposed by Tsiganenko and Usmanov [16] for tail current system simulation is used as a second given field ingredient. The idea of these authors is used here for presentation of the crosstail current as a set of mutually surpassing cylindrically symmetric, straight, infinite current fibers, parallel to the axis Oz (perpendicular to the (x, y) plane). The geometric locus of the points of these fibers, crossing the (x, y) plane is a straight segment, denoted NF. In the work cited NF is placed on the coordinate axis Ox. In contrast, in our consideration NF is permitted to be placed arbitrarily in the (x, y) plane. Another extension of our approach is to allow a linear change along NF of the cross section scale size of these current fibers, denoted by D. As a result, the second given constituent $\tilde{\mathbf{B}}_2$ is constructed in the following way.

The field $\tilde{\mathbf{B}}_2^0$, induced in each point (x, y) of the considered domain by the "fiber" with abscissa x_0, is defined by the formulae

$$B_{2_x}^0(x, y, x_0) = \frac{(y - y_1 - kx_0)(I_1x_0 + I_2)}{(x - x_0)^2 + (y - y_1 - kx_0)^2 + (J_1x_0 + J_2)^2} \tag{22}$$

$$B_{2_y}^0(x, y, x_0) = \frac{(x - x_0)(I_1x_0 + I_2)}{(x - x_0)^2 + (y - y_1 - kx_0)^2 + (J_1x_0 + J_2)^2} \tag{23}$$

$$I_1 = \frac{1}{\pi}\frac{B_F - B_N}{x_F - x_N}; \quad I_2 = \frac{1}{\pi}\left[B_N - x_N\frac{B_F - B_N}{x_F - x_N}\right]$$

$$J_2 = \frac{D_F - D_N}{x_F - x_N}; \quad J_1 = D_N - x_N\frac{D_F - D_N}{x_F - x_N}$$

$$k = \frac{y_N - y_F}{x_N - x_F}; \quad y_1 = y_N - kx_N,$$

where (x_N, y_N) and (x_F, y_F) are the coordinates of the ends of the section NF; B_N and B_F characterize the current density I in the points N and F; $I_j = (c/2\pi)B_j$, $j = N, F$; D_N and D_F are the values of D in points N and F.

The integration of (22), (23) over x_0 from x_N to x_F leads to the final expressions for the magnetic field, induced by the tail current sheet,

$$\tilde{B}_{2_x}(x, y) = \frac{a_1}{b_1}(x_F - x_N) + \frac{b_1a_2 - a_1b_2}{2b_1^2}G(x, y)$$

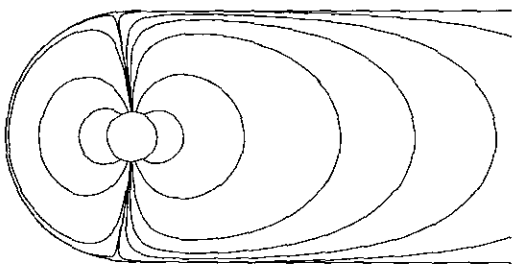

FIG. 3. Closed magnetosphere simulation. The dipole center coordinates are (0, 0). The obtained cusp inclination is 82.7°.

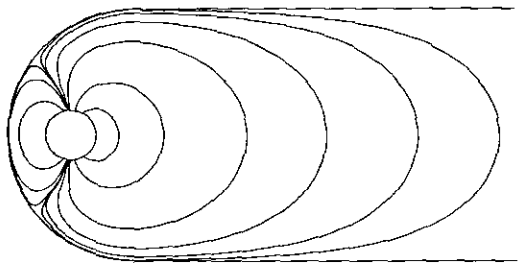

FIG. 4. Closed magnetosphere with dipole, centered at the point (−0.5, 0). The cusp inclination is 63.7°.

$$+\frac{2a_3b_1^2-2a_1b_1b_3-2a_2b_1b_2^2+a_1b_2^2}{2a(x,y)b_1^3}F(x,y) \quad (24)$$

$$\tilde{B}_{2_y}(x,y)=\frac{c_1}{b_1}(x_F-x_N)+\frac{b_1c_2-c_1b_2}{2b_1^2}G(x,y)$$
$$+\frac{2c_3b_1^2-2c_1b_1b_3-c_2b_1b_2+c_1b_2^2}{2a(x,y)b_1^3}F(x,y) \quad (25)$$

$$G(x,y)=\ln\frac{(x_F+b_2/(2b_1))^2+a^2(x,y)}{(x_N+b_2/(2b_1))^2+a^2(x,y)}$$

$$F(x,y)=\arctan\frac{x_F+b_2/(2b_1)}{a(x,y)}-\arctan\frac{x_N+b_2/(2b_1)}{a(x,y)},$$

$$a^2(x,y)=\frac{1}{4}\frac{b_1b_3-b_2^2}{b_1^2},$$

where

$$a_1=-kI_1; \qquad b_1=1+k^2+J_1^2;$$
$$a_2=I_1(y-y_1)-kI_2; \qquad b_2=-2x-2k(y-y_1)+2J_1J_2;$$
$$a_3=I_2(y-y_1); \qquad b_3=x^2+(y-y_1)^2+J_2^2;$$
$$c_1=I_1;$$
$$c_2=I_2-I_1x;$$
$$c_3=-I_2x.$$

It is easy to verify that this field is divergence-free.

4.1.1. *Construction of a Vacuum Magnetosphere Field, a Dipole, and a Magnetopause Shielding Current System*

An initial step of constructing the model of the Earth-type magnetosphere in a sense, given in Section 2, is the vacuum approach, comprising a dipole and a searched field of the magnetopause shielding currents. A grid from Fig. 2 is used in finding the unknown potential, and sets of the type depicted in Fig. 1 are used in the tasks for field line determination (using the procedures, described in Section 3). The arbitrary chosen radius of G here does not correspond to the Earth's radius.

The numerical examples, shown in Figs. 3 and 4 correspond to the closed magnetosphere model. Here the coefficients of (18) are set as

$$\mathcal{C}_L=\mathcal{C}_A=\mathcal{C}_B=\alpha_A=\alpha_B=0. \quad (26)$$

The influence of the displacement O_eL of the dipole, centered at point O_e from the magnetopause subsolar point L on the cusp inclination is demonstrated in the cases of Fig. 3 and Fig. 4. In the geometry accepted here this is equivalent to the influence of the choice of the dayside magnetopause geometry. A closed magnetosphere with zero dipole inclination is considered (270° angle between the Ox-direction and the dipole moment).

The distance O_eL in the case of Fig. 3 is equal to 1 (or $1/2AB$). The obtained cusp inclination is 82.7°.

In the case of Fig. 4, $O_eL = 0.5$. The corresponding cusp inclination is 63.7°.

The next numerical example, reflected in Fig. 5 is an investigation of the expected influence of the interplanetary magnetic field (IMF), parallel to the solar wind velocity. An open magnetosphere is considered. Omitting the discussion, it is quite natural to accept some nonzero normal magnetic field components on the dayside magnetopause, only in this case.

The following values for the parameters are chosen (the dipole, centered in the point (−0.2, 0) is again parallel to Oy):

$$\mathcal{C}_L=0.2\mathcal{B}_{L_T}; \quad \mathcal{C}_A=\mathcal{C}_B=\alpha_A=\alpha_B=0. \quad (27)$$

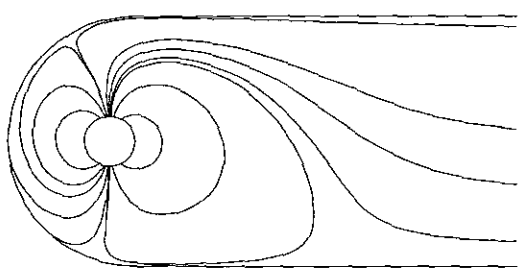

FIG. 5. Simulation of the influence of the x-IMF on the vacuum magnetosphere topology. The normal magnetic field component is supposed to decrease from $\frac{1}{5}$ of the inside value of closed magnetosphere at point L (from Fig. 1) to zero at points A and B.

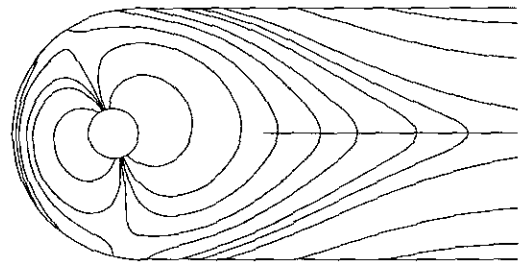

FIG. 6. Magnetosphere magnetic field topology under magnetopause boundary conditions, simulating a northward IMF. A crosstail current sheet, described in Section 4.1.2 (with $y_N = y_F = 0$) is included here as a given internal field, besides the field of the dipole, placed at $(-0.2, 0)$ and tilted by 20°.

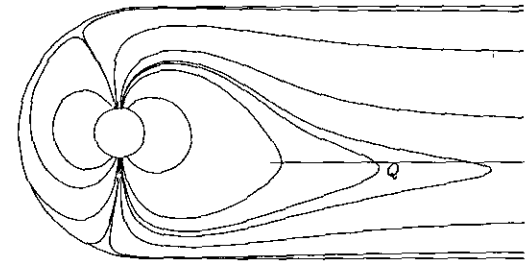

FIG. 7. Magnetic field lines picture, obtained by adding a crosstail current system to the field, shown on Fig. 5. This additional system is placed after an iteration procedure in order to reach the maximum dipole field lines stretching.

One can see on Fig. 5 a strong influence of the x-IMF component on the tail region topology. It has to be recalled that this is only an idealized vacuum model. In a more realistic model, including crosstail currents, this influence is retained as a tendency, but not so sharply expressed (look at the example in Section 4.1.2, Fig. 7).

The next numerical implementation, shown in Fig. 6, demonstrates the possibilities for qualitatively studying, even in the two-dimensional approach, some specific field topology details in the cusp vicinities (here with crosstail currents enclosed; see Section 4.1.2). As is shown in numerous studies [3, 6, 9, 15], some peculiarities of this topology in the case of northward IMF are essential for the explanation of important phenomena of auroral physics.

The parameters, specifying here the boundary conditions (18) reasonably enough as to present the case of northward IMF, are

$$\begin{aligned} &\mathscr{C}_L = 0; \quad \mathscr{C}_A = 0.18\mathscr{B}_{L\tau}; \quad \mathscr{C}_B = -0.18\mathscr{B}_{L\tau}; \\ &\alpha_A = -0.035; \quad \alpha_B = 0.035. \end{aligned} \tag{28}$$

The tile of the dipole, centered at $(-0.2, 0)$, is 20° (290° between Ox and the dipole moment). As a result one can see in Fig. 6 some typical peculiarities around the cusps for the northward IMF field line.

4.1.2. *Including a Crosstail Current Sheet Model*

In order to illustrate the possible self-consistently "fitting" of certain parameters of some given field constituents, an example, described in Fig. 5 (Section 4.1.1), but including now a crosstail current (24), (25), is considered with fixed parameters:

$$B_N = B_F = 0.2\mathscr{B}_{L\tau}; \quad D_F = D_N = 0.2. \tag{29}$$

This parameter selection is not physically substantiated. The goal here is only to apply the above-mentioned iteration procedure for fitting some free parameter (from parameters x_N, y_N; x_F, y_F, i.e., the origin and the end of the "carrying" segment NF, determining the current sheet position). In order to implement such a procedure, heuristic reasons are used for the fitting. It is accepted that

$$x_N = 1.0; \quad x_F = 8.0; \quad NF \| Ox. \tag{30}$$

An appropriate procedure is arranged, fitting $y_N = y_F$ (their equivalence here is supposed) in a way and aiming the maximal stretching of the closed tail field lines such that a convenient closed tail field line s chosen as a test line. In the case considered this is the field line, "starting" from the inner circular cut of the computational domain with polar coordinates relatively near the center of this cut (0.2, 85°). The dependence of the x-coordinate x_Q of the point Q, which is most distant from the dipole (Fig. 7), upon $y_N = y_F$ is shown in Table II. A supposition is made that all remaining parameters of the crosstail current sheet are constants. As expected, x_Q reaches a maximum for some intermediate current sheet position and decreases after removal from this position. As a result the maximum x_Q is reached for $y_N = y_F = -0.24$.

It is seen in Fig. 7 that, as expected, the final displacement of the tail current system, as well as the behavior of the whole field, is ruled by the asymmetry imposed by the dayside boundary conditions (Fig. 5).

The next numerical realization is again a demonstration of the possibility, described in the end of Section 2, for "fitting" some parameters of field ingredient (here the tail current-sheet)

TABLE II

Dependence of the x-Coordinate x_Q of the most Distant from the Dipole Point Q (Fig. 7) upon $y_N = y_F$ for the Test Closed Tail Field Line, Starting from Point with Polar Coordinates (0.2, 85°) Relatively to the Dipole Center

$y_N = y_F$	0.24	0.08	−0.08	−0.16	−0.20	−0.24	−0.28	−0.32	−0.40
x_Q	1.25	1.42	1.59	1.66	1.68	1.69	1.68	1.65	1.60

Note. A supposition is made, that all remaining parameters (29), (30) of the crosstail current sheet are constants.

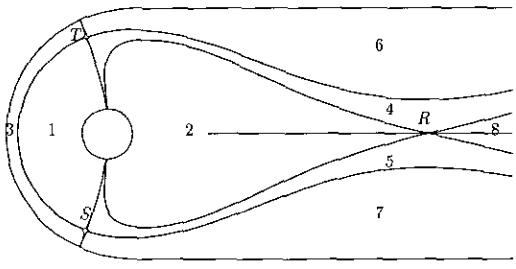

FIG. 8. *Magnetic field topology of an open magnetosphere with zero dipole inclination and boundary conditions, simulating a northward IMF and crosstail current sheet with parameters, given in (31). The topological domains 1–8 are characteristic of these conditions.*

to the field distribution defined by the boundary conditions and other field ingredients.

The picture drawn in Fig. 8 corresponds to the open magnetosphere with zero dipole inclination (dipole centered in point (−0.2, 0)) and boundary conditions simulating a northward IMF and with crosstail current sheet included:

$$\mathcal{C}_L = 0; \quad \mathcal{C}_A = 0.2\mathcal{B}_{L\tau}; \quad \mathcal{C}_B = -0.2\mathcal{B}_{L\tau}; \quad \alpha_A = -0.035;$$
$$\alpha_B = 0.035 \quad x_N = 1.0, \quad x_F = 8.0; \tag{31}$$
$$y_N = y_F = 0; \quad D_F = 0.2 \quad D_N = 0.2.$$

Under these conditions the normal magnetic field component on the magnetopause changes the sign downtail and this circumstance is a cause of the specific topology (with neutral point R). The topological domains 1–8, separated by the field lines, drawn on the figure, are characteristic of these conditions. In varying some tail current sheet parameter, these domains undergo deformations, but do not vanish.

The stationary points T, S, and R on Fig. 8 are solutions of the system

$$\frac{\partial U}{\partial x} + \sum_{i=1}^{2} \tilde{B}_{ix} = 0, \quad \frac{\partial U}{\partial y} + \sum_{i=1}^{2} \tilde{B}_{iy} = 0, \tag{32}$$

where $\tilde{\mathbf{B}}_i$ $i = 1, 2$, are the dipole and the tail current sheet magnetic fields. In the presented implementation the Newton method was used for searching these stationary points.

There are global magnetosphere characteristics, which could be considered and determined (more or less definitely), making use of some additional and independent studies (experiment analysis, theoretical magnetosphere–ionosphere studies, and so on). Such a characteristic may be a position of the neutral point R. Another important additional characteristic could be the magnetic field flux Φ_d across the closed field lines region on dayside (domain 1 on Fig. 8) or the flux Φ_t across the tailside closed field line region (domain 2 on Fig. 8, which could be associated with the closed lines in the plasma sheet) [7, 11]. There could be reasons for searching a solution, leading to a certain position of the point R, to a certain values of Φ_d and Φ_t, or to their ratio $\Lambda = \Phi_d/\Phi_t$.

TABLE III

The Dependence of the Magnetosphere Parameters: Position of R, Dayside (Φ_d), and Tail (Φ_t) Closed Field Lines Field Fluxes, $\Lambda = \Phi_d/\Phi_t$ upon the Parameter $B_N = B_F$ of the Tail Current Sheet (Fig. 8)

β_{sh} ($B_N = B_F = \beta_{sh}\mathcal{B}_{L\tau}$)	x_R	$\Phi_d/\mathcal{B}_{L\tau}$	$\Phi_t/\mathcal{B}_{L\tau}$	Λ
0.00000	2.45179	3.77545	4.75947	0.79351
0.06470	2.43147	3.76805	4.65169	0.81004
0.12941	2.41009	3.76058	4.54558	0.82730
0.19411	2.38752	3.75427	4.41032	0.84534
0.25882	2.33814	3.73783	4.22816	0.88403
0.38822	2.31095	3.73014	4.12271	0.90478
0.45293	2.28176	3.71087	4.01746	0.92369
0.51763	2.25022	3.70175	3.91234	0.94617
0.58234	2.21534	3.68672	3.80749	0.96828

Note. The case parameters are specified in (31).

It is shown in Table III how the variation of one parameter of the tail current sheet ($B_N = B_F = \beta_{sh}\mathcal{B}_{L\tau}$) can affect the position of R (x_R), as well as the dimensionless parameters $\Phi_d/\mathcal{B}_{L\tau}$, $\Phi_t/\mathcal{B}_{L\tau}$, Λ.

4.2. Modeling of Some Possible Features of Uranus Magnetosphere Topology

The last numerical realization reveals a possible approach for qualitative two-dimensional modelling of the magnetosphere of Uranus type, following some early model representations. As was supposed in [19], a possible topology of this magnetosphere, achieved in a certain period of the planet trajectory, could be of unique "pole-on" magnetosphere type, when the dipole moment is almost parallel to the planet–sun line.

This kind of magnetosphere is analyzed in the cited paper, making use of an approach of the magnetohydrostatic equilibrium between thermal plasma and the magnetic field. It is found that the presence of plasma in the tail region, as well as its density and pressure distribution could be described in an acceptable way by a conveniently constructed tail currents system. It is shown there that such a suitable current system is the cylindrical plasma sheet, concentric to the tail boundary cylinder, with its axis aligned to the dipole axis. The currents of this sheet are closed entirely within the tail.

Denote by $N'F'$ and $N''F''$ the sections of the mentioned current cylinder by the plane (x, y). It is quite natural in the two-dimensional presentation to simulate this two-dimensional analog system by two systems of opposite current fibers of the type (24), (25) described above. As in Section 4.1.2, their "carrying" segments $N'F'$ and $N''F''$ are parallel to Ox.

The numerical result, illustrated by the field line picture on

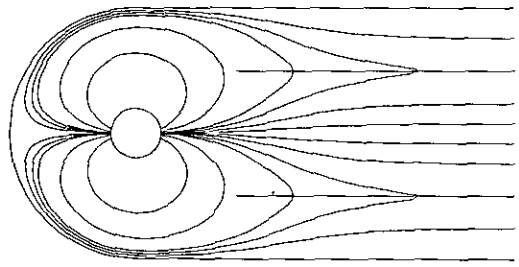

FIG. 9. Simulation of a closed magnetosphere of Uranus type with dipole, directed to Ox. The supposed in the three-dimensional model of Voigt [19] cylindrical current sheet is reflected in our two-dimensional approach by introducing two systems of opposite current fibers of the type (24), (25). Their "carrying" segments $N'F'$ and $N''F''$ (dashed lines on the figure) are parallel to Ox.

Fig. 9 is derived under suppositions close to that of [19, Fig. 1a], after inserting two opposite cross-current systems with parameters:

$$\begin{aligned} &\mathcal{C}_L = \mathcal{C}_A = \mathcal{C}_B = \alpha_A = \alpha_B = 0. \\ &B_{N'} = B_{F'} = 0.1\mathcal{B}_{L\Sigma}; \quad D_{F'} = D_{N'} = 0.06 \\ &B_{N''} = B_{F''} = 0.1\mathcal{B}_{L\Sigma}; \quad D_{F''} = D_{N''} = 0.06 \\ &x_{N'} = 0.8; \quad N'F' \| Ox; \quad |N'F'| = 7.2 \\ &x_{F''} = 0.8; \quad N''F'' \| Ox; \quad |N''F''| = 7.2. \end{aligned} \tag{33}$$

The positions of the current sheets relative to the tail axes are fitted here by an iteration procedure like that in Section 4.1.2, reaching the maximum field line stretching. As a result, $y_{N'} = 0.5$, $y_{N''} = -0.5$.

5. SUMMARY

The physical approach for magnetosphere magnetic field modelling, used in this paper, is well known and widely used in theoretical magnetosphere studies: All the effects connected to the plasma properties and dynamics in this approach are taken into account by introducing some assigned vector fields, or some current systems generating such fields. For the Earth's magnetosphere case these are: dipole field and crosstail currents systems. In this way the searched part of the whole field, possessing a scalar potential, is practically supposed to be in a vacuum approach (divergence-free and curl-free). In the Earth's case this is the field of the magnetopause currents shielding system.

It seems that no direct numerical approaches were used among the different mathematical formalisms solving this problem in the literature.

An appropriate finite element numerical procedure was developed in this paper for solving the boundary value problem so obtained for the Laplace equation in the two-dimensional approach.

The numerical scheme and the applied algorithm for automatic grid generation permits wide flexibility in the selection of the domain geometry and boundary conditions. The algorithm developed for grid and solution transformation, used mainly in the auxiliary procedures in the results' representations could be especially pointed out. In the numerical examples here a two-dimensional analog of the geometry of the earlier Voigt's model [17] is used. Neumann boundary conditions are imposed on the boundary part corresponding to the magnetopause. Under the assumption that the magnetic field tends asymptotically to be parallel to Ox downtail, a special procedure is developed for settling the condition on section CD (Fig. 1). An extension Ω^*, limited by $C'D'$, is considered (Fig. 2) and a Dirichlet condition is imposed on $C'D'$. Solving the problem is implemented repeatedly, lengthening Ω^* until reaching a weak enough influence of this lengthening of the solution on CD.

Several numerical implementations in the paper are chosen rather to demonstrate some capabilities of the numerical procedure than to obtain physical conclusions. Nevertheless, it becomes obvious, that even in this simplified two-dimensional approach, many typical features of the field topology are tentatively illuminated.

An influence of magnetopause geometry on the cusp inclination is demonstrated by replacing the dipole position, maintaining at the same time the remaining geometry problem. The cusp inclination decreases with moving the dipole center toward the subsolar point L.

A north–south magnetosphere tail asymmetry, caused by the interplanetary magnetic field X-component is shown in a vacuum approach. The same tendency of asymmetry is maintained after including a crosstail currents system simulation. A two-dimensional model of this system is proposed in the paper.

A numerical example with boundary conditions, simulating northward IMF, quantitatively demonstrates the possibility of the stirring-type of northward merging.

An example with the magnetic dipole moment aligned to the solar wind flow illustrates a possible flow topology of the "pole-on" magnetosphere of Uranus type. A two-dimensional analog of the cylindrical tail current sheet is proposed.

The development of the described study is planned in several directions. This is, first, elaborating a three-dimensional approach of the problem. On that basis, numerical study of the field topology is obtained as a result of non-trivial boundary normal-component distributions. The theoretical approaches for obtaining such distributions, although not formally connected to the discussed formalism itself, is undoubtedly of a crucial importance. Among the numerous possible implementations of the numerical tool so developed, one can emphasize its usage for modelling the magnetopause electric potential mapping on the polar region.

ACKNOWLEDGMENTS

This research was supported by the Bulgarian National Foundation "Scientific Research" under Contracts 428, F-55, and MM 207/92.

REFERENCES

1. I. I. Alekseev and V. P. Shabansky, *Planet. Space Sci.* **20,** 117 (1972).
2. K. J. Bathe and E. L. Wilson, *Numerical Methods in Finite Element Analysis* (Prentice–Hall, Englewood Cliffs, NJ, 1977).
3. S. W. H. Cowley, *J. Geomag. Geoelectr.* **38,** 1223 (1986).
4. A. I. Fedoseev, V. V. Gusev, M. S. Kaschiev, V. A. Kaschieva, and V. V. Paramonov, *Nucl. Instr. Methods Phys. Res.* **227,** 411 (1984).
5. V. V. Gusev, M. S. Kaschiev, and V. I. Puzinin, Preprint JINR P 11-87-421, Dubna, 1987 (unpublished).
6. J. R. Kan and W. J. Burke, *J. Geophys. Res.* **90,** 4171 (1985).
7. R. L. McPherron, *EOS Transactions. American Geophysical Union* **55,** 994 (1974).
8. S. Pissanetzky, *Sparse Matrix Technology* (Academic Press, London, 1984).
9. P. H. Reiff, *J. Geophys. Res.* **87,** 5976 (1982).
10. J. G. Roederer, *Space Sci. Rev.* **21,** 23 (1977).
11. C. T. Russel, *European Space Agency* **SP-217,** 67 (1984).
12. D. P. Stern, *J. Geophys. Res.* **90,** 10851 (1985).
13. G. Strang and G. Fix, *An Analysis of the Finite Element Method* (Prentice–Hall, Englewood Cliffs, NJ, 1977).
14. F. R. Tofpoletto and T. W. Hill, *J. Geophys. Res.* **94,** 329 (1989).
15. O. A. Troshichev, *J. Atmos. Terr. Prys.* **52,** 1135 (1990).
16. N. A. Tsiganenko and A. V. Usmanov, *Magnetospheric Researches, No. 4 Moscow "Radio i Svlazi," 1984.*
17. G. H. Voigt, *Z. Geophys.* **38,** 319 (1972).
18. G. H. Voigt, *Planet. Space Sci.* **29,** 1 (1981).
19. G. H. Voigt, T. W. Hill, and A. J. Dessler, *Astrophys. J.* **266,** 390 (1983).